

Supporting Information: Dual-carrier Floquet circulator with time-modulated optical resonators

Ian A. D. Williamson,^{*} S. Hossein Mousavi,[†] and Zheng Wang[‡]

Microelectronics Research Center, The University of Texas at Austin, Austin, TX 78758 USA

^{*} Ginzton Laboratory, Stanford University, Stanford, California 94305, USA

[†] Infinera Corporation, 140 Caspian Ct., Sunnyvale, CA 94089, USA

[‡] zheng.wang@austin.utexas.edu

CONTENTS

S1. Frequency Domain Modeling of Periodically Time-Modulated Systems	S3
S2. Coupled-Mode Theory for Floquet Systems	S4
A. Energy Conservation	S6
B. Time Reversal Symmetry	S7
C. Total Scattering Matrix	S8
S3. Dual Floquet Resonators	S9
S4. Analytical Expressions for Scattering Parameters	S10
S5. Nonreciprocal Signal Pathways in Dual-Resonator Circulator	S10
S6. Amplitude Distribution from Full-wave Simulation	S12
S7. Modulated Harmonic Oscillator Stability	S13
S8. Modulated Harmonic Oscillator Solutions	S14
S9. Generation of Compound Multi-Frequency Mode	S14
S10. Modulation Absorption	S16
References	S18

S1. FREQUENCY DOMAIN MODELING OF PERIODICALLY TIME-MODULATED SYSTEMS

Here we outline the approach taken to model the optical Floquet system in the frequency domain. We use a set of single-frequency wave equations which are coupled in the regions that are undergoing modulation. To derive the coupling terms, we start with the general wave equation for the electric field given by

$$\nabla \times \nabla \times \mathbf{E} + \frac{1}{c^2} \frac{\delta^2}{\delta t^2} \mathbf{E} + \frac{1}{\epsilon_0 c^2} \frac{\delta^2}{\delta t^2} \mathbf{P} = 0, \quad (\text{S1})$$

where \mathbf{E} is the total electric field, \mathbf{P} is the total electric polarizability (accounting for both static and modulated terms), ϵ_0 is the vacuum permittivity, and c is the speed of light in vacuum. The refractive index in the modulated region has the form $n'_0 = n_0 + \Delta n_0(t)$ where we assume that the time-varying component is purely sinusoidal,

$$\Delta n_0(t) = \delta n_0 \cos(\Omega t + \phi) = \frac{\delta n_0}{2} \left[e^{j\Omega t} e^{j\phi} + e^{-j\Omega t} e^{-j\phi} \right]. \quad (\text{S2})$$

Eqn. S2 is substituted into Eqn. S1 and the wave equation is rearranged into *static* and *modulated* terms (where $\Delta n_0^2 \ll n_0$) to give

$$\nabla \times \nabla \times \mathbf{E} + \frac{n_0^2}{c^2} \frac{\delta^2}{\delta t^2} \mathbf{E} + \frac{1}{c^2} \frac{\delta^2}{\delta t^2} [2n_0 \Delta n_0(t) \cdot \mathbf{E}] = 0. \quad (\text{S3})$$

By representing the total electric field as a sum of components oscillating at discrete frequencies indexed by n ,

$$\mathbf{E} = \sum_n \mathbf{E}_n e^{j\omega_n t} \quad (\text{S4})$$

and substituting into Eqn. S3, we have

$$\begin{aligned} \nabla \times \nabla \times \mathbf{E}_n e^{j\omega_n t} + \frac{n_0^2}{c^2} \frac{\delta^2}{\delta t^2} \mathbf{E}_n e^{j\omega_n t} + \frac{\delta n_0 n_0}{c^2} \frac{\delta^2}{\delta t^2} \left[\left(e^{j\Omega t} e^{j\phi} + e^{-j\Omega t} e^{-j\phi} \right) \mathbf{E}_n e^{j\omega_n t} \right] = 0 \\ \nabla \times \nabla \times \mathbf{E}_n e^{j\omega_n t} - \frac{\omega_n^2 n_0^2}{c^2} \mathbf{E}_n e^{j\omega_n t} - \frac{\delta n_0 n_0}{c^2} \left[(\omega_n + \Omega)^2 e^{j(\omega_n + \Omega)t + \phi} + (\omega_n - \Omega)^2 e^{j(\omega_n - \Omega)t - \phi} \right] \mathbf{E}_n = 0. \end{aligned} \quad (\text{S5})$$

The expression in Eqn. S5 is an ordinary single-frequency wave equation with an added *nearest-neighbor* coupling term. Essentially, the field oscillating at frequency ω_n feeds energy into the fields oscillating at frequencies $\omega_n \pm \Omega$ through a current distribution proportional to \mathbf{E}_n . The coupling term is,

$$g(n, m) = -\frac{\delta n_0 n_0}{c^2} \omega_n^2 e^{j\phi(n-m)} \delta(|n-m| - 1) \mathbf{E}_m, \quad (\text{S6})$$

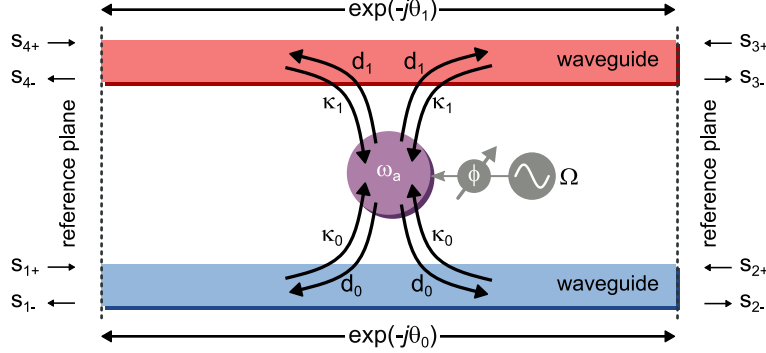


FIG. S1. Schematic of single Floquet resonator with fundamental frequency ω_a modulated at a frequency of Ω and side-coupled to two narrowband waveguides. The coefficients κ_i and d_i represent the structural coupling *into* and *out of* the resonator, respectively. The parameters θ_i represent the phase delay of the waveguides between the port reference planes. The parameter ϕ represents the phase delay is applied to the modulating wave. The complex amplitudes of the incoming and outgoing waves at port n are given by $s_{n\pm}$.

where the $(n - m)$ term in the exponential enforces a negative phase accumulation from a higher-order frequency component to a lower-order frequency component, and a positive phase accumulation from a lower-order frequency component to a higher-order frequency component. The Dirac delta, $\delta(|n - m| - 1)$ enforces the condition of the entire term being non-zero only when n and m differ by 1. This means that with a single-frequency sinusoidal modulation waveform, each frequency component has only two source terms, corresponding to the nearest neighbor frequency components, i.e. $n = 0$ has non-zero terms corresponding to $g(0, -1)$ and $g(0, 1)$.

This coupling can be implemented in finite element analysis by converting to a weak form expression. In this case, the weak form corresponds to a simple multiplication by the test function corresponding to the unknown electric field, e.g. Ψ_n . The following expression can added as a weak contribution in the modulated domain(s) for each frequency component,

$$F_n = g(n, n + 1) \cdot \Psi_n + g(n, n - 1) \cdot \Psi_n. \quad (\text{S7})$$

S2. COUPLED-MODE THEORY FOR FLOQUET SYSTEMS

The coupled-mode theory (CMT) modeling begins by considering only the amplitudes of the Floquet modes that couple to the external environment, in this case $n = 0$ and $n = +1$. The side-coupled resonator system is sketched in Fig. S1 and the frequencies coexist within the same resonator site. The waveguides are configured such that the top waveguide (red) is selective of the $n = +1$ mode and the bottom waveguide (blue) is selective of the $n = 0$ mode. The two

coupled-mode equations that describe the evolution in time of the mode amplitudes are,

$$\frac{d}{dt}u^{(0)}a = (j\omega_a - \gamma)u^{(0)}a + \begin{pmatrix} \kappa_0 & \kappa_0 \end{pmatrix} \begin{pmatrix} s_{1+} \\ s_{2+} \end{pmatrix} \quad (\text{S8})$$

$$\frac{d}{dt}u^{(1)}a = (j\omega_a + j\Omega - \gamma)u^{(1)}a + \begin{pmatrix} \kappa_1 & \kappa_1 \end{pmatrix} \begin{pmatrix} s_{3+} \\ s_{4+} \end{pmatrix} \quad (\text{S9})$$

where s_{m+} is the instantaneous amplitude of the incident wave from the m -th port and $\gamma = \gamma_0 + \gamma_1 + \gamma_L$ for the absorption or radiation rate given by γ_L . All other Floquet modes are maintained at their individual amplitudes dictated by the modulating waveform. The coefficients $\kappa_{0(1)}$ represent the geometric coupling between the incoming wave and the $n = 0 (+1)$ Floquet mode.

The system considered here is distinct from conventional nonreciprocal systems involving Floquet states, because the signal can be carried simultaneously by multiple carriers. To clearly differentiate the signal wave from the carriers, we decompose the instantaneous amplitudes of the incoming and outgoing waves at the m -th port, $s_{m\pm}(\omega) = \tilde{s}_{m\pm}(\Delta)e^{j(\omega_a+n\Omega)t}$ to a slowly varying envelope $\tilde{s}_{m\pm}(\Delta)$, i.e. the signal wave, and the carriers $e^{j(\omega_a+n\Omega)t}$. The instantaneous frequency ω is related to the frequency detuning parameter by $\Delta = \omega - (n\Omega + \omega_a)$ where the integer n is the Floquet order targeted by the particular waveguide or port.

Under this notation, the instantaneous and baseband quantities have the time dependence,

$$a \sim \exp(j\omega t) \quad \tilde{a} \sim \exp(j\Delta t) \quad (\text{S10})$$

$$s_{n\pm} \sim \exp(j\omega t) \quad \tilde{s}_{n\pm} \sim \exp(j\Delta t). \quad (\text{S11})$$

By substituting $d/dt \rightarrow j\omega$, Eqns. S8 and S9 can be combined into a transfer function between the incoming wave amplitudes and the overall modal amplitude given by

$$\tilde{a} = \frac{1}{j\Delta + \gamma} \begin{pmatrix} d_0u^{(0)*} & d_0u^{(0)*} & d_1u^{(1)*} & d_1u^{(1)*} \end{pmatrix} \cdot \begin{pmatrix} \tilde{s}_{1+} \\ \tilde{s}_{2+} \\ \tilde{s}_{3+} \\ \tilde{s}_{4+} \end{pmatrix}, \quad (\text{S12})$$

where d_0 (d_1) represent the structural coupling between the bottom (top) waveguide. The output

CMT equation between the resonator and the ports is

$$\begin{pmatrix} \tilde{s}_{1-} \\ \tilde{s}_{2-} \\ \tilde{s}_{3-} \\ \tilde{s}_{4-} \end{pmatrix} = \begin{pmatrix} 0 & e^{-j\theta_0} & 0 & 0 \\ e^{-j\theta_0} & 0 & 0 & 0 \\ 0 & 0 & 0 & e^{-j\theta_1} \\ 0 & 0 & e^{-j\theta_1} & 0 \end{pmatrix} \begin{pmatrix} \tilde{s}_{1+} \\ \tilde{s}_{2+} \\ \tilde{s}_{3+} \\ \tilde{s}_{4+} \end{pmatrix} + \begin{pmatrix} d_0 u^{(0)} \\ d_0 u^{(0)} \\ d_1 u^{(1)} \\ d_1 u^{(1)} \end{pmatrix} \tilde{a}, \quad (\text{S13})$$

where $\theta_{0(1)} = k_{0(1)}L$ defines the phase shift between the port reference planes in the bottom (top) waveguide for a separation distance given by L . Note that we have assumed the symmetry of the resonator mode results in the same coupling coefficient for port pairs that share a waveguide (i.e. κ_0 , and d_0 for the bottom waveguide and κ_1 and d_1 for the top waveguide). We next use energy conservation and time reversal symmetry to derive the relationships between the linewidth, the coupling coefficients, and the relative Floquet amplitudes.

A. Energy Conservation

We first consider the case of no excitation, meaning that $\tilde{s}_{m+} = 0$ for all m . From Eqns. S8 and S9, this means that

$$\frac{d}{dt} |\tilde{a}|^2 = -2\gamma |\tilde{a}|^2 \quad (\text{S14})$$

and from Eqn. S13, we have

$$-\frac{d}{dt} |\tilde{a}|^2 = \sum |s_{m-}|^2 = \left(2|d_0 \cdot u^{(0)}|^2 + 2|d_1 \cdot u^{(1)}|^2 \right) |\tilde{a}|^2. \quad (\text{S15})$$

By equating the expressions in Eqns. S14 and S15, we conclude that the coupling rates for the bottom and top waveguide to the resonator are given by

$$\gamma_0 = |d_0 \cdot u^{(0)}|^2 \quad (\text{S16})$$

$$\gamma_1 = |d_1 \cdot u^{(1)}|^2 \quad (\text{S17})$$

respectively, where (neglecting radiation and absorption loss) the total linewidth is $\gamma = \gamma_0 + \gamma_1$. When absorption or radiation loss is negligible ($\gamma_L \ll \gamma_0, \gamma_1$), an ideal nonreciprocal response occurs at critical coupling ($\gamma_0 = \gamma_1$), which is equivalent to the condition

$$\left| \frac{d_0}{d_1} \right| = \left| \frac{u^{(1)}}{u^{(0)}} \right|. \quad (\text{S18})$$

An important consequence of Eqn. S18 is that any difference in the relative amplitudes of the two modes can be compensated by structurally asymmetric coupling (quantified by the ratio $|d_0|/|d_1|$) to achieve the ideal on-resonance response.

B. Time Reversal Symmetry

The first condition provided by time reversal symmetry is

$$2\gamma = 2\kappa_0 d_0^* + 2\kappa_1 d_1^*, \quad (\text{S19})$$

which, when taken with Eqn. S16 and Eqn. S17, implies that $\kappa_m = d_m |u^{(m)}|^2$. Additionally, the direct scattering process through the waveguides requires that

$$\begin{pmatrix} d_0 \\ d_0 \\ d_1 \\ d_1 \end{pmatrix} = - \begin{pmatrix} 0 & e^{-j\theta_0} & 0 & 0 \\ e^{-j\theta_0} & 0 & 0 & 0 \\ 0 & 0 & 0 & e^{-j\theta_1} \\ 0 & 0 & e^{-j\theta_1} & 0 \end{pmatrix} \begin{pmatrix} d_0^* \\ d_0^* \\ d_1^* \\ d_1^* \end{pmatrix}, \quad (\text{S20})$$

or equivalently, $d_0 = -e^{-j\theta_0} d_0^*$ and $d_1 = -e^{-j\theta_1} d_1^*$. By selecting the location of the reference planes such that θ_0 and θ_1 are some integer multiple of 2π , the expression in Eqn. S20 is satisfied by d_0 and d_1 being purely imaginary and with magnitudes that satisfy Eqns. S17. The complete expressions are therefore

$$d_0 = j \frac{\sqrt{\gamma_0}}{|u^{(0)}|} \quad (\text{S21})$$

$$d_1 = j \frac{\sqrt{\gamma_1}}{|u^{(1)}|} \quad (\text{S22})$$

$$\kappa_0 = d_0 |u^{(0)}|^2 = j\sqrt{\gamma_0} |u^{(0)}| \quad (\text{S23})$$

$$\kappa_1 = d_1 |u^{(1)}|^2 = j\sqrt{\gamma_1} |u^{(1)}|. \quad (\text{S24})$$

C. Total Scattering Matrix

Combining Eqn. S12 and the output coupling relationship given by Eqn. S13, leads to a scattering matrix for the single-Floquet resonator system as a function of the detuning,

$$\begin{aligned}
\tilde{a} &= \frac{1}{j\Delta + \gamma} \begin{pmatrix} \kappa_0 & \kappa_0 & \kappa_1 & \kappa_1 \\ u^{(0)} & u^{(0)} & u^{(1)} & u^{(1)} \end{pmatrix} \cdot \begin{pmatrix} \tilde{s}_{1+} \\ \tilde{s}_{2+} \\ \tilde{s}_{3+} \\ \tilde{s}_{4+} \end{pmatrix} \\
&= \frac{1}{j\Delta + \gamma} \begin{pmatrix} \frac{d_0 |u^{(0)}|^2}{u^{(0)}} \\ \frac{d_0 |u^{(0)}|^2}{u^{(0)}} \\ \frac{d_1 |u^{(1)}|^2}{u^{(1)}} \\ \frac{d_1 |u^{(1)}|^2}{u^{(1)}} \end{pmatrix}^T \cdot \begin{pmatrix} \tilde{s}_{1+} \\ \tilde{s}_{2+} \\ \tilde{s}_{3+} \\ \tilde{s}_{4+} \end{pmatrix} \\
&= \frac{1}{j\Delta + \gamma} \begin{pmatrix} j\sqrt{\gamma_0} e^{-j\angle u^{(0)}} \\ j\sqrt{\gamma_0} e^{-j\angle u^{(0)}} \\ j\sqrt{\gamma_1} e^{-j\angle u^{(1)}} \\ j\sqrt{\gamma_1} e^{-j\angle u^{(1)}} \end{pmatrix}^T \cdot \begin{pmatrix} \tilde{s}_{1+} \\ \tilde{s}_{2+} \\ \tilde{s}_{3+} \\ \tilde{s}_{4+} \end{pmatrix}. \tag{S25}
\end{aligned}$$

The output coupling is given by the relationship

$$\begin{aligned}
\begin{pmatrix} \tilde{s}_{1-} \\ \tilde{s}_{2-} \\ \tilde{s}_{3-} \\ \tilde{s}_{4-} \end{pmatrix} &= \begin{pmatrix} 0 & e^{-j\theta_0} & 0 & 0 \\ e^{-j\theta_0} & 0 & 0 & 0 \\ 0 & 0 & 0 & e^{-j\theta_1} \\ 0 & 0 & e^{-j\theta_1} & 0 \end{pmatrix} \begin{pmatrix} \tilde{s}_{1+} \\ \tilde{s}_{2+} \\ \tilde{s}_{3+} \\ \tilde{s}_{4+} \end{pmatrix} + \begin{pmatrix} d_0 u^{(0)} \\ d_0 u^{(0)} \\ d_1 u^{(1)} \\ d_1 u^{(1)} \end{pmatrix} \tilde{a} \\
&= \begin{pmatrix} 0 & e^{-j\theta_0} & 0 & 0 \\ e^{-j\theta_0} & 0 & 0 & 0 \\ 0 & 0 & 0 & e^{-j\theta_1} \\ 0 & 0 & e^{-j\theta_1} & 0 \end{pmatrix} \begin{pmatrix} \tilde{s}_{1+} \\ \tilde{s}_{2+} \\ \tilde{s}_{3+} \\ \tilde{s}_{4+} \end{pmatrix} + \begin{pmatrix} j\sqrt{\gamma_0} e^{j\angle u^{(0)}} \\ j\sqrt{\gamma_0} e^{j\angle u^{(0)}} \\ j\sqrt{\gamma_1} e^{j\angle u^{(1)}} \\ j\sqrt{\gamma_1} e^{j\angle u^{(1)}} \end{pmatrix} \tilde{a}. \tag{S26}
\end{aligned}$$

By combining Eqn. S25 with Eqn. S26 and letting $\phi = \angle u^{(1)} - \angle u^{(0)}$, the complete scattering matrix for the system can be solved for,

$$S^I(\Delta) = \begin{pmatrix} 0 & 1 & 0 & 0 \\ 1 & 0 & 0 & 0 \\ 0 & 0 & 0 & 1 \\ 0 & 0 & 1 & 0 \end{pmatrix} - \frac{1}{j\Delta + \gamma} \begin{pmatrix} \gamma_0 & \gamma_0 & \sqrt{\gamma_0\gamma_1} e^{-j\phi} & \sqrt{\gamma_0\gamma_1} e^{-j\phi} \\ \gamma_0 & \gamma_0 & \sqrt{\gamma_0\gamma_1} e^{-j\phi} & \sqrt{\gamma_0\gamma_1} e^{-j\phi} \\ \sqrt{\gamma_0\gamma_1} e^{j\phi} & \sqrt{\gamma_0\gamma_1} e^{j\phi} & \gamma_1 & \gamma_1 \\ \sqrt{\gamma_0\gamma_1} e^{j\phi} & \sqrt{\gamma_0\gamma_1} e^{j\phi} & \gamma_1 & \gamma_1 \end{pmatrix}. \tag{S27}$$

Note that the superscript I in S^I denotes the case of a single Floquet resonator.

S3. DUAL FLOQUET RESONATORS

In the frame of the individual waveguide ports, the dual-resonator Floquet system is characterized by the following set of coupled mode equations

$$\frac{d}{dt} \begin{pmatrix} \tilde{a}_1 \\ \tilde{a}_2 \end{pmatrix} = H \begin{pmatrix} \tilde{a}_1 \\ \tilde{a}_2 \end{pmatrix} + K \begin{pmatrix} \tilde{s}_{1+} & \tilde{s}_{2+} & \tilde{s}_{3+} & \tilde{s}_{4+} \end{pmatrix}^T \quad (\text{S28})$$

$$\begin{pmatrix} \tilde{s}_{1+} \\ \tilde{s}_{2+} \\ \tilde{s}_{3+} \\ \tilde{s}_{4+} \end{pmatrix} = C \begin{pmatrix} \tilde{s}_{1+} \\ \tilde{s}_{2+} \\ \tilde{s}_{3+} \\ s_{4+} \end{pmatrix} + D \begin{pmatrix} \tilde{a}_1 \\ \tilde{a}_2 \end{pmatrix}, \quad (\text{S29})$$

where \tilde{a}_1 and \tilde{a}_2 denote the slowly varying envelopes of the modes in the left and the right resonator, respectively and ϕ_a and ϕ_b are their associated modulation phases. The self- and inter-resonator coupling matrix is

$$H = \begin{pmatrix} j\omega_a & j\mu \\ j\mu & j\omega_b \end{pmatrix} - \begin{pmatrix} \gamma & \gamma_0 e^{-j\theta_0} + \gamma_1 e^{-j\theta_1} e^{j(\phi_b - \phi_a)} \\ \gamma_0 e^{-j\theta_0} + \gamma_1 e^{-j\theta_1} e^{j(\phi_a - \phi_b)} & \gamma \end{pmatrix}, \quad (\text{S30})$$

the input port coupling matrix is

$$K = \begin{pmatrix} j\sqrt{\gamma_0} & j\sqrt{\gamma_0} e^{-j\theta_0} & j\sqrt{\gamma_1} e^{-j\theta_1} e^{-j\phi_a} & j\sqrt{\gamma_1} e^{-j\phi_a} \\ j\sqrt{\gamma_0} e^{-j\theta_0} & j\sqrt{\gamma_0} & j\sqrt{\gamma_1} e^{-j\phi_b} & j\sqrt{\gamma_1} e^{-j\theta_1} e^{-j\phi_b} \end{pmatrix}, \quad (\text{S31})$$

the output port coupling matrix is

$$D = \begin{pmatrix} j\sqrt{\gamma_0} & j\sqrt{\gamma_0} e^{-j\theta_0} \\ j\sqrt{\gamma_0} e^{-j\theta_0} & j\sqrt{\gamma_0} \\ j\sqrt{\gamma_1} e^{-j\theta_1} e^{j\phi_a} & j\sqrt{\gamma_1} e^{j\phi_b} \\ j\sqrt{\gamma_1} e^{j\phi_a} & j\sqrt{\gamma_1} e^{-j\theta_1} e^{j\phi_b} \end{pmatrix}, \quad (\text{S32})$$

and the direct port-to-port scattering matrix is

$$C = \begin{pmatrix} 0 & e^{-j\theta_0} & 0 & 0 \\ e^{-j\theta_0} & 0 & 0 & 0 \\ 0 & 0 & 0 & e^{-j\theta_1} \\ 0 & 0 & e^{-j\theta_1} & 0 \end{pmatrix}. \quad (\text{S33})$$

θ_0 and θ_1 are the transmission phases of the bottom and top waveguide shown in Fig. S1. Note that $D \neq K^T$ and $\gamma = \gamma_0 + \gamma_1 + \gamma_L$. Throughout this work we assume that the two resonators are structurally identical ($\omega_b = \omega_a$) and that evanescent coupling between the two resonator sites is negligible ($\mu = 0$). The full scattering matrix as a function of the detuning frequency is

$$S^{II}(\Delta) = C + D \cdot \left[\begin{pmatrix} j\Delta & 0 \\ 0 & j\Delta \end{pmatrix} - H \right]^{-1} \cdot K \quad (\text{S34})$$

where the superscript II denotes a cascade of two Floquet resonators.

S4. ANALYTICAL EXPRESSIONS FOR SCATTERING PARAMETERS

Considering the relationship $\theta_0 = \theta_1 + \Delta\theta$, the condition for ideal isolation between α_O and β_O is

$$e^{2j\theta_0} (e^{j\Delta\theta} - j) (je^{j\Delta\theta+2j\theta_0} + e^{2j\Delta\theta+2j\theta_0} - je^{j\Delta\theta} - 1) = 0 \quad (\text{S35})$$

which is satisfied by $\Delta\theta = \pi/2$, independently of the value of θ_0 . Ideal operation between β_E and α_O translates to a slightly different expression given by

$$-e^{2j\theta_0} (e^{j\Delta\theta} - j) (e^{2j(\Delta\theta+\theta_0)} - je^{j(\Delta\theta+2\theta_0)} + je^{j\Delta\theta} - 1) = 0 \quad (\text{S36})$$

which is satisfied by the same condition $\Delta\theta = \pi/2$. The overall dispersive scattering matrix of the system becomes a circulator response given by

$$S_c^{II} = \begin{pmatrix} -\frac{\gamma}{\gamma+j\Delta} & -\frac{j\gamma\Delta}{(\gamma+j\Delta)^2} & 0 & \frac{\Delta^2}{(\Delta-j\gamma)^2} \\ 0 & 0 & 1 & 0 \\ 0 & \frac{j\Delta}{\gamma+j\Delta} & 0 & -\frac{\gamma}{\gamma+j\Delta} \\ \frac{j\Delta}{\gamma+j\Delta} & \frac{\gamma^2}{(\gamma+j\Delta)^2} & 0 & -\frac{j\gamma\Delta}{(\gamma+j\Delta)^2} \end{pmatrix}. \quad (\text{S37})$$

The scattering matrix in Eqn. S37 is distinct from the scattering response of a three-port junction circulator [S1], where transmission in one of the forward direction has the form

$$T = \frac{2}{3} \left(\frac{e^{j4\pi/3}}{1 + j(\omega - \omega_a)/\gamma_a} + \frac{e^{j2\pi/3}}{1 + j(\omega - \omega_b)/\gamma_b} \right). \quad (\text{S38})$$

S5. NONRECIPROCAL SIGNAL PATHWAYS IN DUAL-RESONATOR CIRCULATOR

The on-resonance operation of the Floquet circulator can be visualized by tracing a compound mode as it travels through the system and becomes transformed by the segments of waveguides

and as it reflects and transmits through the resonators (Fig. S2). For the $\beta_E \rightarrow \alpha_O$ path, the signal enters as the even mode on the right, and is transformed into the circular mode, by the dual-waveguide segment between the resonator and the ports on the right. This circular mode, perfectly transmits through the right resonator (as shown in Fig. 2d of the main text with $\phi = \pi/2$). Propagation down the middle waveguide segment transforms the signal into the odd mode, which then impinges on the left resonator and is perfectly transmitted out the other side (as shown in Fig. 2b of the main text with $\phi = 0$). Note that the complete forward transmission from $\beta_E \rightarrow \alpha_O$ is due to the lack of coupling to either resonator, which holds even when the input signal is off-resonance. As a result, the forward transmission is unitary regardless of the detuning as expected from the expression in Eqn. S37. The backward transmission is resonantly suppressed, with a 30 dB isolation bandwidth of $\sim 0.07\gamma$. Such broadband complete transmission in the forward direction is spectrally distinct from that of conventional junction circulators.

Transmission along the $\alpha_O \rightarrow \beta_O$ path can be analyzed similarly, with multiple reflections between the two resonators before the signal emerges (Fig. S2). This pair of ports provides a $70\times$ larger isolation bandwidth ($\sim 5\gamma$) than the previous pair, but at a cost of reduced forward transmission off-resonance. Ultimately, γ and the associated operating bandwidth is limited by the fundamental frequency of the modulating wave and the and the propagation of the coupling waveguides. The remaining ports in the system do not participate in any cross-device scattering pathways: the even mode on the left resonantly reflects into itself $\alpha_E \rightarrow \alpha_E$, and the even mode on the right resonantly reflects into the odd mode on the right $\beta_O \rightarrow \beta_E$.

On-resonance this results in the response

$$S_c^{\text{II}}(\Delta = 0) = \begin{pmatrix} -1 & 0 & 0 & 0 \\ 0 & 0 & 1 & 0 \\ 0 & 0 & 0 & -1 \\ 0 & 1 & 0 & 0 \end{pmatrix}, \quad (\text{S39})$$

while off-resonance the scattering is reciprocal with the response

$$S_c^{\text{II}}(\Delta \rightarrow \infty) = \begin{pmatrix} 0 & 0 & 0 & 1 \\ 0 & 0 & 1 & 0 \\ 0 & 1 & 0 & 0 \\ 1 & 0 & 0 & 0 \end{pmatrix}. \quad (\text{S40})$$

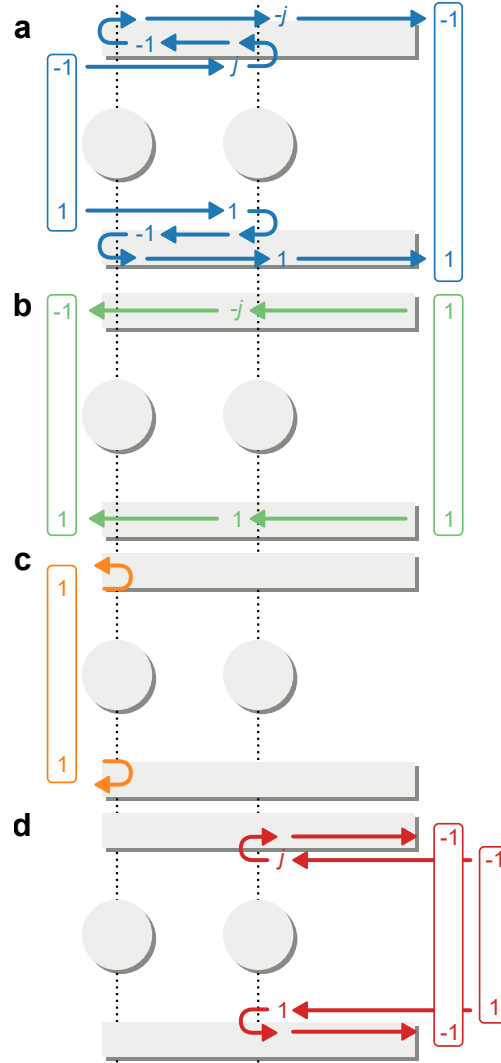


FIG. S2. (a) Incidence of odd mode from the left undergoes two reflections before being resonantly transmitted out of the right side. (b) Incidence of the even mode from the right is non-resonantly transmitted to the odd mode on the left. (c) Incidence of the even mode from the left is resonantly reflected back into the even mode. (d) Incidence of the odd mode from the right is resonantly reflected back into the even mode on the right.

S6. AMPLITUDE DISTRIBUTION FROM FULL-WAVE SIMULATION

In purely sinusoidal phase modulation, the distribution of the Floquet amplitudes is given by the Jacobi-Anger expansion [S2]. Fig. S3 plots the amplitude distribution inside one of the modulated photonic crystal resonators (from Fig. 4 of the main text) at steady state when excited on resonance. The simulation includes a total of seven frequency components, but the configuration of the system (Fig. 1) allows only the $n = 0$ and $n = +1$ bands to couple into and out of the

system.

Note that the amplitudes shown in Fig. S3 are normalized to the fundamental $n = 0$ amplitude.

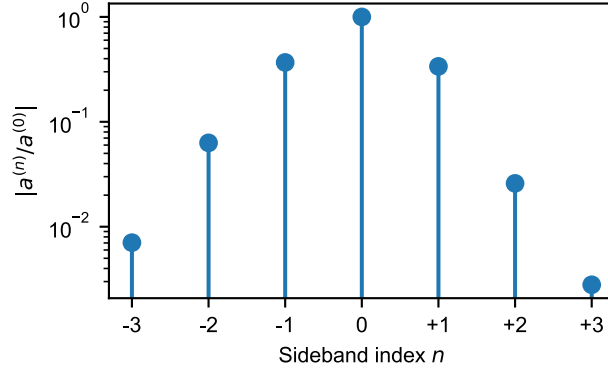


FIG. S3. Sideband amplitude distribution in the left resonator of the photonic crystal circulator implementation. The distribution was numerically computed in COMSOL Multiphysics under on-resonance excitation of the compound even mode from the left port.

S7. MODULATED HARMONIC OSCILLATOR STABILITY

Neglecting damping, the Floquet resonator considered in this work is equivalent to a parametrically modulated harmonic oscillator, which obeys the Mathieu differential equation. In dimensionless form this is given by [S3, S4]

$$\frac{\delta^2 a}{\delta t^2} + [1 + \delta \cos(\Omega t)] a = 0, \quad (\text{S41})$$

where a is the oscillator amplitude, δ is the modulation index, and Ω is the modulation rate. This equation admits stable and unstable periodic solutions depending on the combination of modulation parameters. A map of the stability regions has been computed and is given in Figure S4 where the dark blue regions correspond to unstable solutions that occur due to parametric resonance when the system is driven at harmonics of the fundamental system resonance. In this work we limit consideration to relatively *weak* and *slow* modulation which corresponds to the region around the origin (bottom left) of Figure S4.

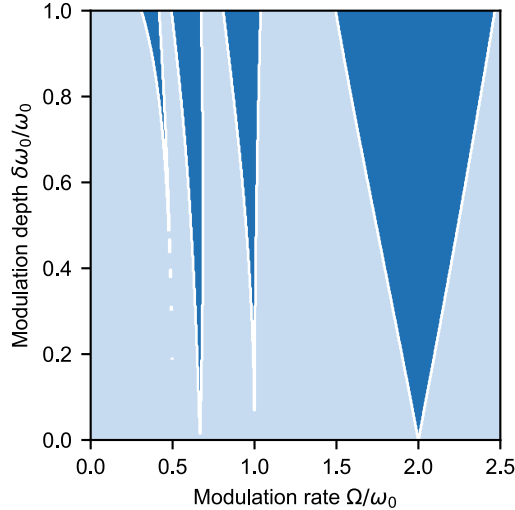


FIG. S4. Modulated harmonic oscillator stability map. (light blue) Stable and (dark blue) unstable solutions as a function of modulation rate and modulation depth.

S8. MODULATED HARMONIC OSCILLATOR SOLUTIONS

As discussed in the main text, more general forms of periodic modulation, beyond the case of a sinusoid with a single frequency, can facilitate the control over mode amplitudes. For example, a modulation waveform that includes a second harmonic component, meaning that it has frequency components of Ω and 2Ω , supports an amplitude distribution where the $n = +1$ and $n = +2$ Floquet modes have the same amplitude, i.e. $u^{(1)} = u^{(2)}$ as shown in Fig. S5.

S9. GENERATION OF MULTI-FREQUENCY MODE

The compound multi-frequency mode can be generated with the three port optical circuit shown in Figure S6. The signal incident through port one can be resonantly converted into the compound mode defined over ports two and three. This implementation requires that $\gamma_0 = \gamma_1 + \gamma_2$ which can be achieved through structural and Floquet mode engineering. For example, the Floquet amplitude distribution in Fig. S6b could be used.

Not that this system is reciprocal in that it can also operate in the reverse direction. Incidence of the even mode from the right will be resonantly converted into the single-carrier mode on the left.

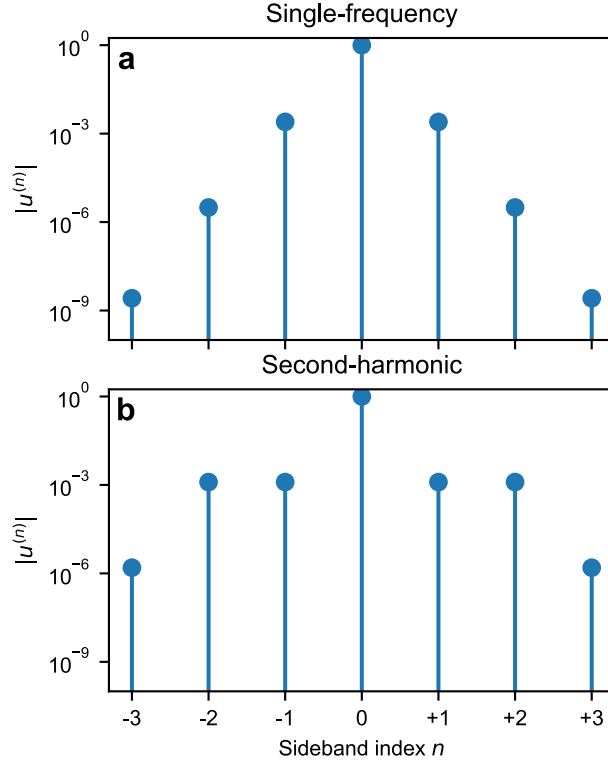


FIG. S5. Floquet mode amplitude distributions for single frequency and second harmonic parametric modulation. Single frequency modulation (left) has modulation of the form $f(t) = 1 + \delta \cos(\Omega t)$ and second harmonic (right) has the form $f(t) = 1 + \delta_1 \cos(\Omega t) + \delta_2 \cos(2\Omega t)$ where $\delta_2 = 2\delta_1$. Sideband amplitudes were computed by numerically solving Eqn. S41 using the harmonic balance method [S3, S4].

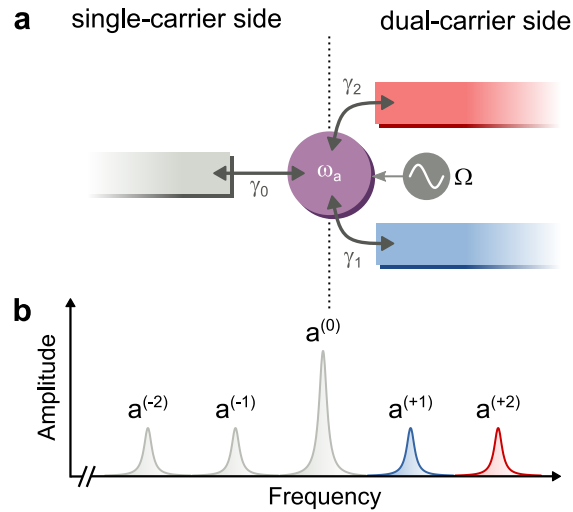


FIG. S6. Compound multi-frequency mode generation. (a) Schematic of a three-port compound mode generator. (b) Sideband distribution that would be compatible with the structure in (a).

S10. MODULATION ABSORPTION

The photonic crystal Floquet circulator discussed in the main text demonstrates the operating principals using full-wave physics but neglects material absorption from modulation. To present a complete picture of the system performance, in this section we characterize the losses that would result from carrier injection and depletion in silicon. This is the strongest mechanism available in silicon, but other approaches and material systems could be the subject of future study.

The associated resonator absorption rate is calculated from an eigenmode simulation of the photonic crystal resonator with a dielectric loss tangent applied to the defect rod. The applied loss tangent is converted into a change in refractive index through the carrier concentrations reported in [S5]. As shown by the dashed border of gray region in S7a, the resulting absorption rate overwhelms the waveguide coupling rates $\gamma_L \gg \gamma_0, \gamma_1$ and means that slight adjustment of the system is needed for practical operation.

One option for overcoming the losses is to increase the structural coupling factors, fitted from the system in Fig. 5 as $d_0 = 1.2 \times 10^{-3}$ and $d_1 = 4 \times 10^{-3}$. This situation is shown in Fig. S7b where the coefficients have been increased to $d_0 = 1.8 \times 10^{-2}$ and $d_1 = 6 \times 10^{-2}$ which can be achieved by removing a photonic crystal lattice constant separating the resonator and waveguides. However, this results in a resonator quality factor that's reduced by a factor of $\sim 10^2$, and requires that other aspects of the system be reconfigured. For example, both the modulation frequency and CROW bandwidth would need to be enlarged in order to meet the requirement of one-to-one coupling between Floquet states and waveguides.

As discussed in the main text, more general periodic modulation waveforms can be used to provide additional degrees of freedom for tuning the coupling. As shown in Fig. S7c, a amplitude distribution with equal amplitudes in $u^{(1)}$ and $u^{(2)}$ can be used. By reconfiguring the top and bottom waveguide to couple to $u^{(2)}$ and $u^{(1)}$, respectively, the modulation index can be used to tune only the total quality factor. This approach achieves critical coupling between the waveguides and the resonators for a wide range of modulation index because γ_0 and γ_1 as a function of modulation index overlap. Increasing the structural coupling coefficients d_n would shift the curve for overlapping γ_0 and γ_1 in Fig. S7c further to the left. This means that the circulator can operate with a *total* linewidth comparable to the one in the simulated photonic crystal, a practical modulation frequency, and low loss.

In terms of the isolation and insertion loss performance, the absorption impacts the two cross-device scattering pathways in different ways (Fig. S8). As γ_L becomes comparable to γ_0 and γ_1 , the

$\alpha_O \rightarrow \beta_O$ pathway experiences higher insertion loss but maintains a very high level of isolation. However, the $\beta_E \rightarrow \alpha_O$ pathway experiences reduced isolation for larger γ_L with no penalty in insertion loss.

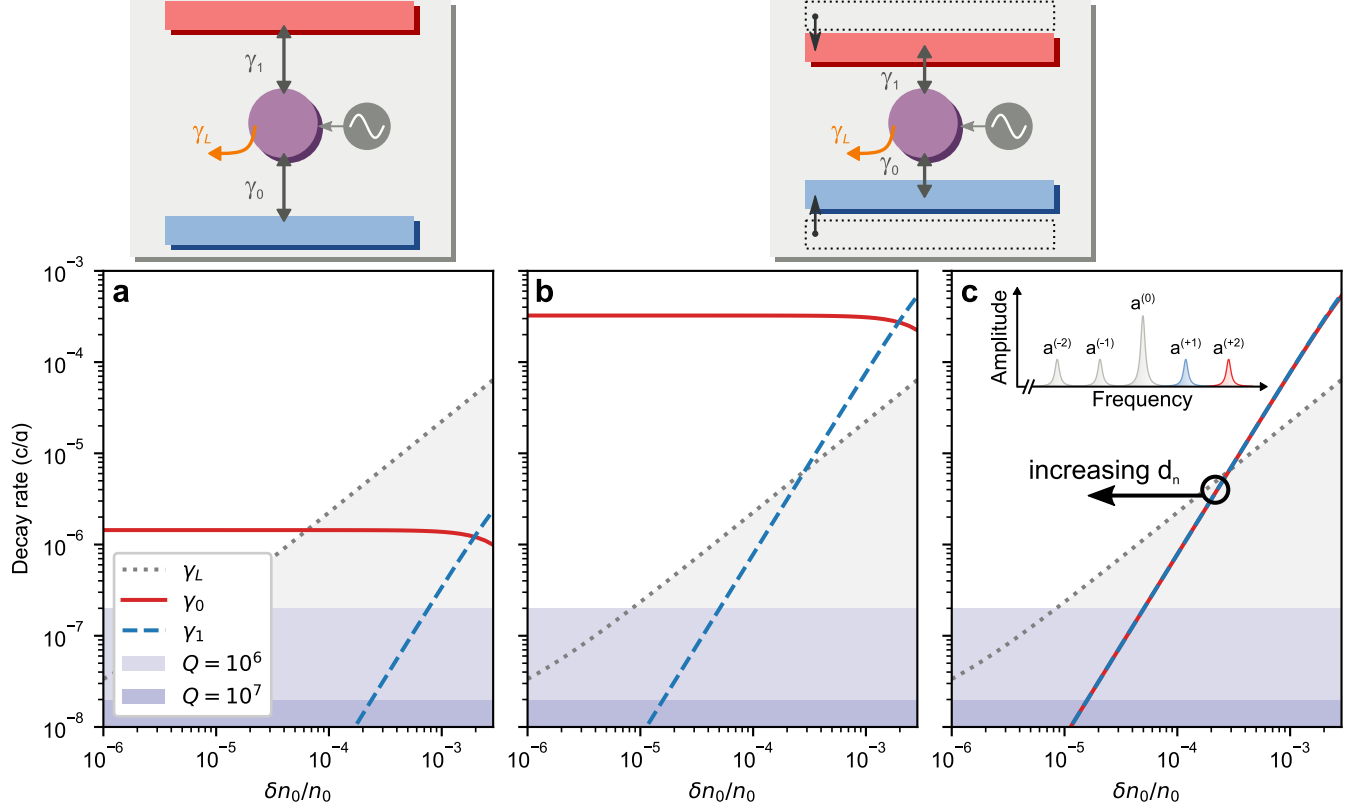


FIG. S7. Resonator decay rates to bottom waveguide γ_0 , top waveguide γ_1 , and absorption γ_L . The top edges of the shaded regions represent the decay rates associated with an out-of-plane quality factor of 10^6 and 10^7 , demonstrating that the typical values achieved in photonic crystal slab resonators will not overwhelm the circulator response. The absorption rate (dashed border of gray region) is the intrinsic decay rate calculated from an eigenmode simulation of the photonic crystal point defect. A dielectric loss tangent is applied to the simulated defect rod and by assuming modulation takes place through the plasma dispersion effect in silicon, the loss tangent was converted into a relative change in refractive index through the carrier concentrations reported in [S5]. (a) Decay rates from fitting to photonic crystal simulation where $d_0 = 1.2 \times 10^{-3}$ and $d_1 = 4 \times 10^{-3}$. (b) Configuration where d_0 and d_1 have been increased to $d_0 = 1.8 \times 10^{-2}$ and $d_1 = 6 \times 10^{-2}$. (c) Configuration where $d_0 = 1.8 \times 10^{-2}$ and $d_1 = 6 \times 10^{-2}$ and the top and bottom waveguides have been configured to use the first- and second-order Floquet states shown in the inset, where $u^{(1)} = u^{(2)}$. In this configuration γ_0 and γ_1 are overlapping and critical coupling is achieved for many possible modulation strengths. Further increasing the structural coupling coefficients d_n will shift the curve to the left.

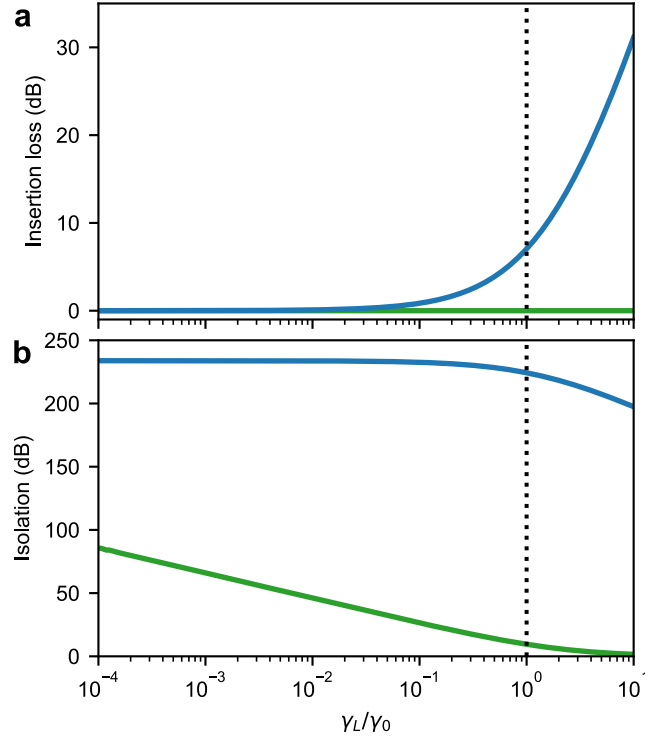


FIG. S8. (a) Insertion loss and (b) isolation in the $\alpha_O \rightarrow \beta_O$ (blue) and $\beta_E \rightarrow \alpha_O$ (green) scattering pathways as a function of the resonator loss rate, normalized to the coupling rate to the bottom waveguide. The $\alpha_O \rightarrow \beta_O$ pathway experiences large insertion loss for higher γ_L but maintains large isolation. On the other hand, the $\beta_E \rightarrow \alpha_O$ pathway experiences reduced isolation for higher γ_L but no increased insertion loss.

[S1] B. Lax and K. J. Button, *Microwave Ferrites and Ferrimagnetics* (McGraw-Hill, 1962).

[S2] A. Yariv, *Quantum Electronics* (Wiley, 1989).

[S3] N. McLachlan, *Theory and Application of Mathieu Functions* (Clarendon Press, 1947).

[S4] G. Acar and B. F. Feeny, *Journal of Vibration and Acoustics* **138**, 041017 (2016).

[S5] R. Soref and B. Bennett, *IEEE Journal of Quantum Electronics* **23**, 123 (1987).